Carbohydrate Polymers 87 (2012) 598–606

Contents lists available at SciVerse ScienceDirect

Carbohydrate Polymers

journal homepage: www.elsevier.com/locate/carbpol

Debranched cassava starch crystallinity determination by Raman spectroscopy: Correlation of features in Raman spectra with X-ray diffraction and ^{13}C CP/MAS NMR spectroscopy

Christopher Mutungi[a,*], Lars Passauer[b], Calvin Onyango[c], Doris Jaros[a], Harald Rohm[a]

[a] Institute of Food Technology and Bioprocess Engineering, Technische Universitaet Dresden, D-01062 Dresden, Germany
[b] Institute of Plant and Wood Chemistry, Technische Universitaet Dresden, D-01737 Tharandt, Germany
[c] Food Technology Division, Kenya Industrial Research and Development Institute, P.O. Box 30650-00100, Nairobi, Kenya

ARTICLE INFO

Article history:
Received 16 June 2011
Received in revised form 9 August 2011
Accepted 11 August 2011
Available online 19 August 2011

Keywords:
Starch
Crystallinity
X-ray diffraction
^{13}C CP/MAS NMR
Raman spectroscopy

ABSTRACT

Because starch crystallinity influences the physical, mechanical, and technological aspects of numerous starch-based products during production and storage, rapid techniques for its assessment are vital. Samples of different levels of crystallinity were obtained by debranching gelatinized cassava starch, followed by subjection to various hydrothermal treatments. The recrystallized products were further subjected to partial hydrolysis with a mixture of α-amylase and glucoamylase prior to freeze–drying. Crystallinities were determined using X-ray diffraction (XRD) and ^{13}C CP/MAS NMR spectroscopy, and correlated with FT-Raman spectra features. XRD crystallinities ranged between 0 and 58%, and agreed with crystalline-phase fractions (R^2 = 0.99) derived from the respective ^{13}C CP/MAS NMR spectra. A strong linear correlation was found between crystallinities and integrated areas of the skeletal mode Raman band at 480 cm^{-1} (R^2 = 0.99). With appropriate calibration, FT-Raman spectroscopy is a promising tool for rapid determination of starch crystallinity.

1. Introduction

Starch, the main storage polysaccharide in plants, is widely used in food, feed, pharmaceutical and other industrial applications. Amylose and amylopectin are the main constituent polymers. These are arranged systematically to form semi-crystalline granules that exhibit a degree of crystallinity of 15–45% (Tester, Karkalas, & Qi, 2004). Because of this semi-crystalline structure, native starch granules give X-ray diffraction patterns which have been used to categorize starches into A-, B- and C-polymorphs (Imberty, Buleon, Tran, & Perez, 1991). Generally, cereal starches belong to A-polymorph whereas tuber and amylose-rich starches belong to B-polymorph. Legume and some tuber starches are categorized as C-polymorph (Tester et al., 2004).

The crystalline orientation of starch has been extensively studied (Tester et al., 2004). A- and B-polymorphs arise from left-handed parallel double-helical strands assembled in monoclinic and hexagonal lattice symmetries, respectively (Imberty et al., 1991). A higher density of packing of double helices, and fewer water molecules in the interstices of the A-polymorph as compared to the B-polymorph is the main structural difference between the two polymorphs. The C-polymorph is formed when both A- and B-polymorphic arrangements co-exist. Another crystalline arrangement, the V-form, is also categorized, but is based on single-helical glucopyranosyl chains (Buleon, Veronese, & Putaux, 2007). These crystalline forms also appear when gelatinized starch recrystallizes under different conditions (Buleon et al., 2007; Mutungi, Rost, Onyango, Jaros, & Rohm, 2009).

Starch crystallinity affects the physical, mechanical, and technological properties of numerous starch-based products, and is therefore relevant for product development, quality and process control. In foods, loss of native crystallinity via gelatinization influences apparent viscosity, gelation and matrix forming characteristics, whereas reordering of the starch during processing or storage has impact product texture, stability, quality, digestibility and functionality (Sajilata, Singhal, & Kulkarni, 2006). In pharmaceutical applications, starch may be used as an excipient. A certain degree of crystallinity is desired for the starch to maintain specific drug release and other functional properties (Pifferi, Santoro, & Pedrani, 1999). In tablet formulation, for example, changes in crystallinity can occur during production processes such as drying, granulation, coating, compression, and milling because of exposure to mechanical stress, temperature changes, and different humidity levels. Amorphization or crystalline transformation can also occur during storage. The variations may modify properties such as compressibility or flowability or induce changes in

* Corresponding author. Tel.: +49 351 463 36943; fax: +49 351 463 37126.
E-mail address: chrismutungi@yahoo.co.uk (C. Mutungi).

0144-8617/$ – see front matter © 2011 Elsevier Ltd. All rights reserved.
doi:10.1016/j.carbpol.2011.08.032

solubility, dissolution or bioavailability of the active ingredient (de Veij, Vandenabeele, De Beer, Remonc, & Moens, 2009). For these reasons techniques for the assessment of starch crystallinity are fundamentally relevant, especially if they offer possibilities rapid testing.

Infrared (IR) absorption spectroscopy has been used to follow starch crystallinity and molecular order because some spectral bands respond to these structural aspects (van Soest, Tournois, deWit, & Vliegenthart, 1995). However, intensities of IR absorption bands are highly masked by intense absorption of water molecules, and are therefore poorly resolved. This effect renders quantitative interpretation of signals difficult. An alternative to IR-spectroscopy is Raman spectroscopy, which like IR-spectroscopy also probes vibrational transitions taking place in the ground electronic state of molecules. The method (Raman spectroscopy) measures the fraction of incident photon, usually monochromatic light from a visible or near infrared laser, which is scattered at an altered energy state due to vibrational transition energy of a molecule. The Raman signal is thus dependent on changes in polarizability of functional groups, whereas IR absorption signal is dependent on intrinsic dipole moment changes as the molecule vibrates (Ma & Phillips, 2002).

Raman spectroscopy exhibits minimal interference from moisture because water is only weakly polarizable. For this reason, numerous other bands typical of starch become apparent in the spectra, and can be evaluated (Thygesen, Lokke, Micklander, & Engelsen, 2003). A number of studies have investigated the Raman signal of starch in response to molecular order loss during gelatinization (Kim, Yeh, Zhao, & Wang, 1989; Schuster, Ehmoser, Gapes, & Lendl, 2000) and molecular order gain during retrogradation (Bulkin, Kwak, & Dea, 1987; Fechner, Wartewig, Kleinebudde, & Neubert, 2005; Ma & Phillips, 2002). Other investigators have also used Raman spectroscopy to detect differences in native (Dupuy & Laureyns, 2002; Santha, Sudha, Vijayakumari, Nayar, & Moorthy, 1990; Wellner, Georget, Parker, & Morris, 2011), chemically-modified (Dupuy & Laureyns, 2002; Passauer, Bender, & Fischer, 2010; Phillips, Xing, Chong, Liu, & Corke, 2000), and physically-modified starches (Kizil, Irudayaraj, & Seetharaman, 2002). To the best of our knowledge, no discrete attempts have been made to correlate Raman signals with the long-range order of starch although spectra obtained for B- and V-amylose (Cael, Koenig, & Blackwell, 1973) indicated that the technique is sensitive to conformational differences. Aim of this study was to investigate the extent to which Raman spectra relate to crystallinity of starch substrates as determined by wide angle X-ray diffraction, and solid-state ^{13}C cross-polarization and magic angle spinning nuclear magnetic resonance (^{13}C CP/MAS NMR) spectroscopy.

2. Materials and methods

2.1. Preparation of starch samples

Starch samples of different crystallinities were prepared from cassava starch. A 10% (w/w) starch–water mixture was autoclaved at 121 °C for 15 min, and the cooled gel (50 °C) incubated with pullulanase (Sigma P2986, Sigma–Aldrich, Laborchemikalien GmbH, Steinheim, Germany) as described elsewhere (Mutungi, Onyango, Jaros, Henle, & Rohm, 2009). The debranched starch (DS) was freeze–dried, and the powder subjected to various recrystallization conditions: annealing (ANN), temperature-cycling (TC) or heat-moisture treatment (HMT). ANN-DS preparation involved autoclaving a 20% (w/w) DS-water mixture at 121 °C for 15 min followed by incubation of the gel in a water-bath at 60 °C for 24 h. Preparation of TC-DS was done by subjecting a similar mixture to three autoclaving (121 °C for 2 h) and incubation cycles (60 °C for 1 h in the first two cycles, and 60 °C for 16 h in the third cycle). HMT-DS was prepared by moistening DS to 30% (w/w) moisture content and autoclaving the wetted powder at 121 °C for 2 h. Portions of ANN-DS, TC-DS and HMT-DS were also subjected to a partial hydrolysis protocol, involving treatment with a solution of α-amylase (Sigma A3176) and amylogucosidase (Sigma A7095) at 37 °C for 16 h in a sodium acetate-hydrochloric acid buffer (pH 5.2), containing 0.02% sodium azide (Mutungi et al., 2011). The partially digested samples were labelled dANN-DS, dTC-DS and dHMT-DS, respectively. All samples were freeze–dried and finely ground using motor and pestle.

2.2. Wide angle X-ray diffraction (XRD)

A Siemens D5000 (Bruker-AXS, Karlsruhe, Germany) X-ray diffractometer was used. Samples were scanned with Cu Kα radiation ($\lambda = 0.154$ nm), and reflections were detected in the angular range $2\theta = 5–37.5°$ with a step intervals of 0.01°. Scanning duration at each step was 6.5 s. The X-ray generator operating conditions were 40 kV and 25 mA. An amorphous sample prepared by autoclaving a 10% (w/w) cassava starch–water suspension followed by freeze drying after storage at −82 °C for 20 min, was also scanned for background scattering estimation.

2.3. Nuclear magnetic resonance spectroscopy

Solid-state ^{13}C CP/MAS NMR measurements were performed on a Bruker Avance 300 spectrometer (Bruker BioSpin, Karlsruhe, Germany) operating at 75.48 MHz for the ^{13}C nucleus. A commercial double resonance 4 mm MAS NMR probe was used, and a ramped $^{1}H–^{13}C$ cross-polarization applied. Sample spectra were accumulated with a spinning rate of 14 kHz at the magic angle (54.7°). The cross-polarization contact time was 4 ms with a recycle delay of 2 s. Spectra were acquired with a line broadening of 10 Hz. At least 2000 scans were accumulated for each spectrum at room temperature. Spinal ^{1}H-decoupling was applied during signal acquisition to remove proton spin–spin interactions and improve spectra resolution. Spectra were referenced indirectly to a zero value for tetramethylsilane. Quantitative evaluation of spectra involved decomposition of each spectrum into the respective amorphous- and ordered-phase signatures by subtracting a linearly scaled spectrum of the amorphous starch sample so that the intensity of the difference (ordered-phase) sub-spectrum was zero at 84 ppm (Paris, Bizot, Emery, Buzare, & Buleon, 1999). Scaling of the amorphous spectrum and spectral subtraction were done on Microsoft Excel® solver. The ordered-phase sub-spectra were then fitted with deconvolution peaks, and integrated areas of peaks within the C1 atom signal were used in calculation of crystalline-phase contents. PeakFit® version 4.12 was used for spectra processing.

2.4. Fourier transform-Raman spectroscopy (FT-Raman)

Raman spectra were recorded on a Bruker MultiRAM FT-Raman spectrometer (Bruker Optics, Ettlingen, Germany) equipped with an air-cooled neodymium-doped yttrium aluminium garnet (Nd:YAG) laser source operating at $\lambda_{Nd:YAG} = 1064$ nm, and a liquid nitrogen-cooled germanium diode detector. Samples were placed on an aluminium holder and 200 scans were accumulated and co-added. The spectral resolution was 4 cm^{-1}. Evaluation of acquired spectra involved integrating band areas, band widths, and wavenumber at maximum height of bands in the region 3500–300 cm^{-1} after baseline correction and vector normalization against the C–O–C symmetric stretch mode at ~865 cm^{-1} using the manufacturer's software OPUS/QUANT version 6.

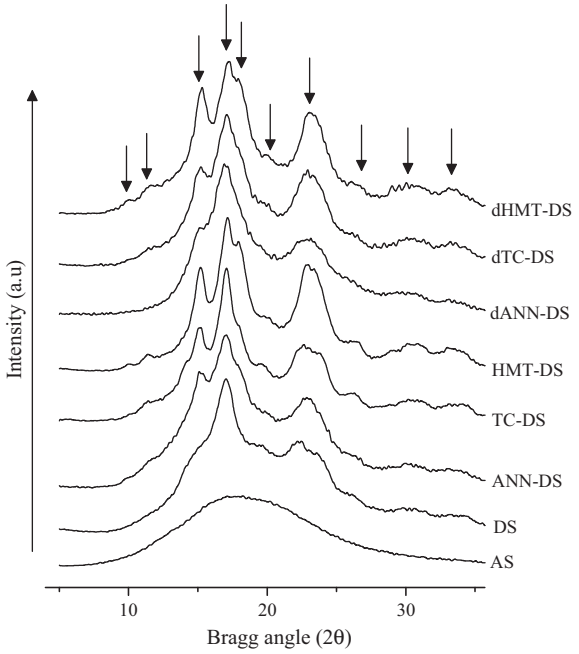

Fig. 1. X-ray diffractograms of amorphous starch (AS), debranched starch (DS), annealed debranched starch (ANN-DS), temperature-cycled debranched starch (TC-DS), heat-moisture treated debranched starch (HMT-DS), and the partially digested forms: dANN-DS, dTC-DS and dHMT-DS.

3. Results and discussion

3.1. XRD crystallinity

Aqueous starch re-associates by forming double-helical strands along the linear sections of constituent polymer chains. These strands subsequently aggregate to ordered domains of different morphologic orientation depending on recrystallization conditions (Buleon et al., 2007). One way to increase starch recrystallization is by debranching it with enzymes that hydrolyze α-(1→6) bonds in the amylopectin, and in some amylose chains (Mutungi, Onyango, et al., 2009; Pohu, Planchot, Putaux, Colonna, & Buleon, 2004). However, recrystallization of starch is a complex process involving conformational change, chain alignment, crystal packing, and phase propagation (Bulkin et al., 1987). Whereas debranching frees short linear α-(1→4) polymers that favor crystallization, the longer amylose chains associate much faster and form networks that impede propagation of substantially ordered crystallites. Enhancement of recrystallization is achieved by subjecting the debranched starch to hydrothermal treatments (Mutungi, Rost, et al., 2009). The effects of various hydrothermal conditions classified as annealing, temperature cycling and heat-moisture treatment were reported in an earlier investigation (Mutungi, Rost, et al., 2009); the different combinations of thermal and plasticization conditions induce chain ordering effects that result in products of different crystallinity and crystalline orientations.

Fig. 1 shows X-ray diffractograms of the various starch preparations. Evolution patterns, and intensities of individual reflections particularly at $2\theta = \sim 10^\circ$, 11°, 15°, 17°, 18°, 20°, 23°, 24°, 26°, 30°, and 33° indicate that the materials comprise mainly different contents of A-, and B-polymorphs, and small amounts of V-type structures. A-polymorph is frequently distinguished by strong reflections at $2\theta = 15.11^\circ$, 17.14°, 18.14°, and 26.27°, with some additional reflections at $2\theta = 9.98^\circ$, 11.19°, 22.93°, 23.68°, 30.30° and 33.08° (Lopez-Rubio, Flanagan, Gilbert, & Gidley, 2008), whereas B-polymorph is recognized by typical reflections at $2\theta = 5.51^\circ$, 14.60° and 16.85° with auxiliary peaks at

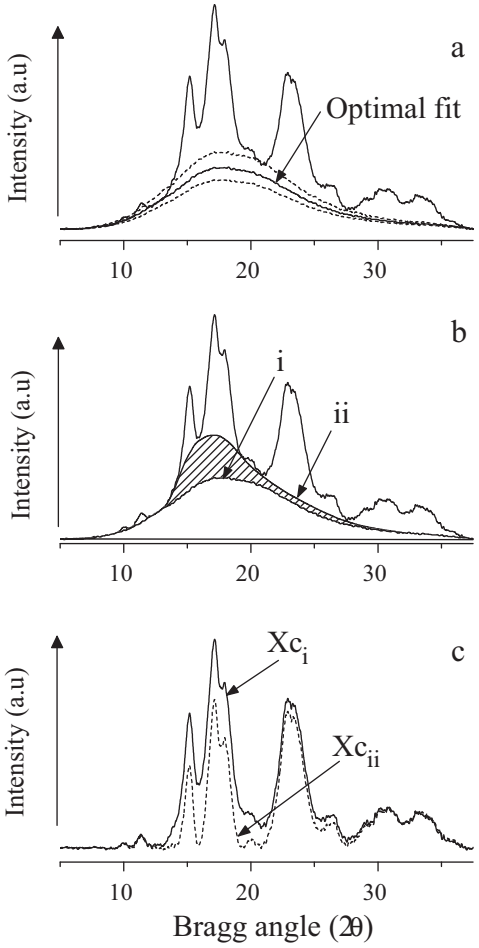

Fig. 2. Amorphous-template fitting on sample XRD diffractogram (a), decomposition of diffractogram by amorphous-template baseline [i] or by diffractogram-minima baseline [ii] fitting (b), and the difference spectra representing crystalline fractions, Xc_i and Xc_{ii}, by the two approaches, respectively (c). Shaded region in (b) represents diffuse scattering by imperfect and small crystallites.

$2\theta = 10.01^\circ, 11.02^\circ, 13.85^\circ, 22.30^\circ, 23.71^\circ, 26.16^\circ, 30.61^\circ$ and 33.84°. V-polymorph is identified by a reflection at $2\theta = 19.8^\circ$ and occasionally, additional reflections occur at $2\theta = 7.4^\circ$ and 13.0° (Lopez-Rubio et al., 2008).

HMT and dHMT subscribe more to A-type crystallinity especially because the respective diffractograms exhibit a clear A-polymorph signature doublet at $2\theta = 17.1^\circ$ and 18.1° in addition to strong reflections at $2\theta = 15.1^\circ$. The rest of the samples are varying mixtures of A- and B-polymorphs (C-polymorph) because the respective XRD patterns neither exhibit the A-polymorph signature doublet ($2\theta = 17.1^\circ$ and 18.1°) nor the B-polymorph signature reflection, which is usually a strong peak at $\sim 2\theta = 5.5^\circ$ (Cairns, Bogracheva, Ring, Hadley, & Morris, 1997). The reflection at $2\theta \approx 20^\circ$ is low, and indicates that only small amounts of V-type structures are regularly packed so as to diffract X-rays. Furthermore, some intensity at this angular position can also arise from A- or B-crystalline packing (Lopez-Rubio et al., 2008).

From the intensities of reflections (arrows Fig. 1) the various samples exhibit different crystallinity levels. A common method used to quantify crystallinity of starch involves fitting a smooth curve under the main minima of diffractograms (Fig. 2), as originally proposed by Hermans and Weidinger (1948) for cellulose. The method assumes a two-phase situation, whereby relatively perfect crystalline domains are interspersed in an amorphous background, so that crystallites give distinct reflections. However, ordered starch often exhibits imperfections in the form of chain foldings,

entangled chain ends, or branched-chain segments that are constrained within crystallite assemblies (Lopez-Rubio et al., 2008). These non-crystalline interfaces cause fluctuations in the relative distances between corresponding atoms in the ideal lattice, and therefore some scattering ability of crystallites is lost or becomes diffuse. Furthermore, small crystallites that possess only a few lattice planes may not produce sufficiently detectable reflection intensities. This diffuse intensity is erroneously estimated together with the amorphous background when the two-phase approach is adopted (Gernat, Radosta, Anger, & Damaschun, 1993; Lopez-Rubio et al., 2008).

To improve accuracy of crystallinity estimation, Lopez-Rubio et al. (2008) proposed a method for modeling the amorphous contribution by fitting a Gaussian profile to the experimental diffractogram. Whereas the approach could account for lattice imperfections, a baseline derived from an appropriate amorphous template is easier to fit, and also corrects for instrumental background scattering as well (Cairns et al., 1997). In Fig. 2, profiles of diffractogram-minima baseline and amorphous-template baseline fittings are illustrated. The amorphous template is fitted under the sample diffractogram with respect to the two extreme ends, so that no negative intensities are generated on the difference sub-diffractogram upon subtraction. Clearly the amorphous scattering does not extend up to the base of diffraction peaks as projected by the diffractogram-minima baseline. Intensity difference between the diffractogram-minima baseline and the amorphous-template baseline (Fig. 2b) may be taken as measure of diffuse scattering arising from imperfect and small crystallites. The crystallinity values calculated using the two approaches are presented in Table 1.

Crystallinity increased in the order DS < ANN-DS < TC-DS < HMT-DS in both approaches, and values obtained by the amorphous-template approach were substantially higher. However, for the partially hydrolyzed samples, that is, dANN-DS, dTC-DS, and dHMT-DS, derived from ANN-DS, TC-DS, and HMT-DS, respectively, the amorphous-template approach revealed an increase in crystallinity in each case (dANN-DS > ANN-DS; dTC-DS > TC-DS and dHMT-DS > HMT-DS), whereas the diffractogram-minima baseline approach gave lower crystallinity values (dANN-DS < ANN-DS; dTC-DS < TC-DS and dHMT-DS < HMT-DS). This disagreement is explained by the fact that diffractogram-minima baseline approach does not account for diffuse scattering, which might have increased in the partially hydrolyzed samples due to crystallite erosion and disentanglement of packed chains during enzyme action (Mutungi et al., 2011). Furthermore, a less rigid chain packing in the hydrolyzed samples is especially implied by the loss of reflection intensities at $2\theta = 15^\circ$ and 18° (Fig. 1). Strong reflections in these angular positions typify the more dense A-type crystalline structure.

3.2. Crystalline-phase by ^{13}C CP/MAS NMR

Starch polymers in crystalline and non-crystalline assemblies possess different α-(1→4) glycosidic bond torsion angles. This implies different local electron densities around carbon atoms in the different domains due to conformational effects (Paris et al., 1999). The different conformational populations can be probed using solid-state ^{13}C CP/MAS NMR because a straight forward correlation exists between chain conformation and the peak profile of the C1 atom resonance signal (Gidley & Bociek, 1988; Paris, Bizot, Emery, Buzare, & Buleon, 2001). Regularly arranged conformations of crystalline packed chains correspond to narrow resonance frequency C1 bands with multiplicities determined by space group equivalent symmetry classes, whereas chain conformations that are not crystalline become sufficiently distorted on an average so as not to show up at similar chemical shifts (Paris et al., 1999). By deconvolution of the C1 signal, chains that are packed into crystalline domains, and those that are not, can thus be conveniently delineated (Mutungi et al., 2011; Paris et al., 2001). Moreover, the intensity of the C4 atom signal relates directly to the content of the amorphous phase in a sample (Gidley & Bociek, 1988).

^{13}C CP/MAS spectra of the different starches are shown in Fig. 3. Spectral consistency was tested by evaluating the intensity ratio between the combined intensities of C2, C3, C4 and C5 resonance signals and the intensity of C1 resonance signal (Paris et al., 1999; Tan, Flanagan, Halley, Whittaker, & Gidley, 2007). This ratio was 3.97 ± 0.12 for the different samples spectra, and the constancy provided confidence that the amorphous and crystalline regions behaved fairly similarly with respect to their solid state nature as probed by the NMR experiment. The intensity of C4 signal progressively decreased in the order AS > DS > ANN-DS > TC-DS > HMT-DS, signifying decreasing amount of the amorphous-phase, and was indistinct among the partially digested substrates (i.e. dANN-DS, dTC-DS and dHMT-DS). These findings are in agreement with the XRD crystallinities derived using the amorphous-template approach reported in Table 1, which depict increase in crystallinity following partial hydrolysis of the materials. Amorphous- and ordered-phases were quantified by decomposing NMR spectra based on the assumption that each individual spectrum is a linear combination of amorphous- and ordered-phase signatures (Paris et al., 1999). An example of spectrum decomposition and the resultant sub-spectra is illustrated in Fig. 4. Amorphous-phase content was calculated from the C1 signal (90–107 ppm) as percent ratio of the difference in integrated intensity before and after spectrum decomposition relative to the integrated intensity before decomposition. The values are presented in Table 1. Amorphous-phase contents were not determined for dANN-DS, dTC-DS, dHMT-DS as the C4 signal was too weak in these samples (Fig. 3). Lack of distinct signals at the C4 chemical shift region indicated that the amorphous fraction in the partially digested samples was hydrolyzed by amylolytic enzymes, resulting in increased molecular ordering of the remaining crystalline fraction (Mutungi et al., 2011).

In Fig. 3, profiles of the deconvoluted C1 atom signals are also illustrated. The two sets of peak multiplicities, a triplet and a doublet, characteristic of A- and B-crystalline packing, respectively, are evident. A triplet appears in A-type starch because double helices packed in the typical monoclinic lattice, depict three equivalent classes for the six monomers that constitute a single helical turn; the three classes correspond to three distinct torsions about the α-(1→4) linkage. A doublet, on the contrary, appears in B-crystalline packing for the reason that two equivalent classes of α-(1→4) bond torsions are exhibited among the hexagonally packed chain duplexes (Paris et al., 1999). The multiplicity sets produce narrow line contributions at approximately 99, 100 and 101 ppm (intensity ratio 1:1:1) and at about100 and 101 ppm (intensity ratio 1:1). For this reason, crystalline-phase was calculated from the relative intensity contribution of these lines in the C1 atom signal of the ordered-phase sub-spectra as illustrated in Fig. 4c. Once a doublet or triplet was assigned, three other peaks representing contributions related to interfacial conformations were allocated at approximately 94, 97 and 103 ppm as discussed elsewhere (Mutungi et al., 2011; Paris et al., 2001). In comparison to Gaussian and Lorentzian functions, Voigt function provided the most reproducible fitting of peaks with approximately equal intensities for the triplet or doublet. The Voigt function combines both Gaussian and Lorentzian profiles and is defined by the equation:

$$y = f \cdot \frac{\lambda}{\pi} \int_{-\infty}^{\infty} \frac{\exp(-t^2)}{\lambda^2 + (\sigma - t)^2}\, dt$$

where $f = (1/w_G)(\ln 2)^{1/2}$; $\lambda = (w_L/w_G)(\ln 2)^{1/2}$; $\sigma = ((x - x_c)/w_G)(\ln 2)^{1/2}$; and w_G and w_L are full width at half maximum (FWHM) of the Gaussian and the Lorentzian profiles,

Table 1
XRD crystallinity (%), and relative proportions of structural phases (%) by ^{13}C CP/MAS NMR.

Sample	XRD crystallinity (Xc)		Structural phase		
	Xc_i[a]	Xc_{ii}[b]	Amorphous	Crystalline	Interfacial
AS	0	0	100	nd	nd
DS	19.0 ± 1.3[c]	33.4 ± 1.3	49.9 ± 1.5	30.6 ± 0.8	19.4 ± 0.8
ANN-DS	23.9 ± 0.2	40.9 ± 3.2	33.9 ± 1.6	41.7 ± 2.5	24.4 ± 3.4
TC-DS	36.3 ± 1.7	50.7 ± 3.1	28.3 ± 2.3	52.2 ± 1.5	19.5 ± 2.0
HMT-DS	41.7 ± 1.7	56.2 ± 1.4	20.4 ± 1.8	56.0 ± 2.2	23.6 ± 3.5
dANN-DS	21.8 ± 0.5	47.9 ± 1.2	nd	50.9 ± 4.0	48.7 ± 2.5
dTC-DS	30.8 ± 0.9	54.4 ± 1.1	nd	56.9 ± 3.1	43.1 ± 2.5
dHMT-DS	33.4 ± 1.4	58.2 ± 2.4	nd	61.3 ± 3.0	37.1 ± 3.5

AS: amorphous starch; DS: debranched starch; ANN-DS: annealed debranched starch; TC-DS: temperature-cycled debranched starch; HMT-DS: heat-moisture treated debranched starch; dANN-DS, dTC-DS and dHMT-DS are partially digested forms of ANN-DS, TC-DS and HMT-DS, respectively; nd: not determined.
[a] Diffractogram-minima baseline approach.
[b] Amorphous-template baseline approach.
[c] Means ± standard deviation of four independent fitting procedures.

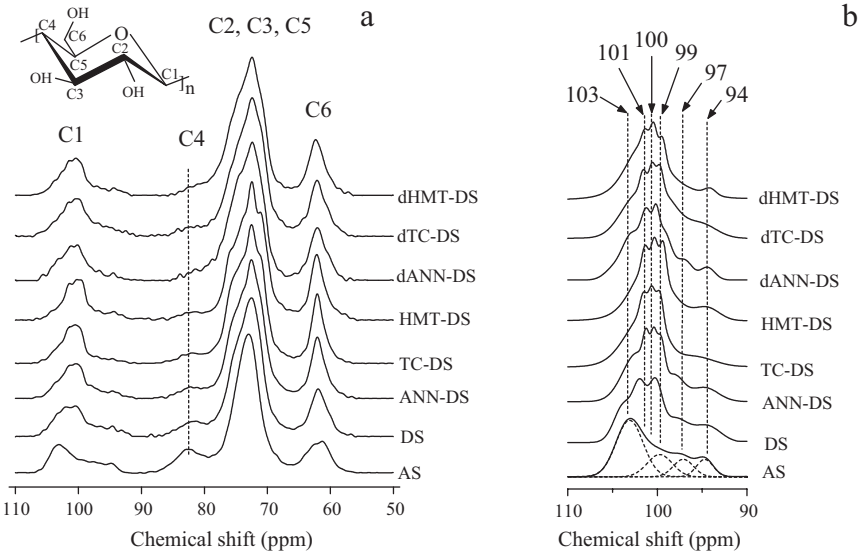

Fig. 3. ^{13}C CP/MAS NMR spectra of amorphous starch (AS), debranched starch (DS), annealed debranched starch (ANN-DS), temperature-cycled debranched starch (TC-DS), heat-moisture treated debranched starch (HMT-DS), and the partially digested forms: dANN-DS, dTC-DS and dHMT-DS. Broken line in (a) marks C4 atom signal associated with amorphous phase. (b) Deconvoluted profiles of the C1 atom signals; broken lines mark polymorph related peak multiplicities [101, 100 and 99 ppm], and displacements arising from interfacial-phase contributions [103, 97 and 94 ppm].

respectively, x_c is the centre and t is integral parameter. Contributions by crystalline- and interfacial-phases in the various starches, expressed as percent fraction relative to the total integrated intensity of the C1 signal before spectral decomposition are given in Table 1. NMR crystalline-phase contents closely correspond to the XRD crystallinities derived by the amorphous-template baseline approach. The latter data (XRD crystallinities by amorphous-template fitting) were correlated with Raman spectra features, and only these have been referenced to in the subsequent discussion.

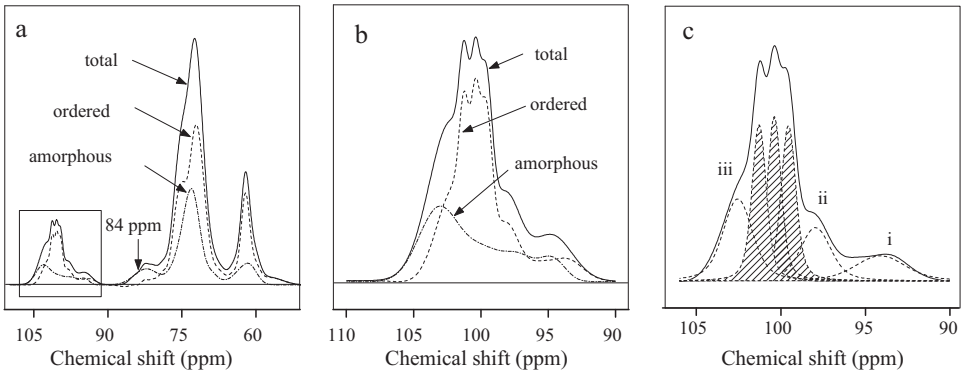

Fig. 4. ^{13}C CP/MAS NMR spectrum decomposition into amorphous and ordered phases ((a) and (b)), and deconvolution of the ordered-phase C1 signal (c). Intensity of shaded peaks (triplet in A- and doublet in B-type starch) represent crystalline fraction. Intensities i, ii and iii are interfacial-phase contributions in the ordered-phase.

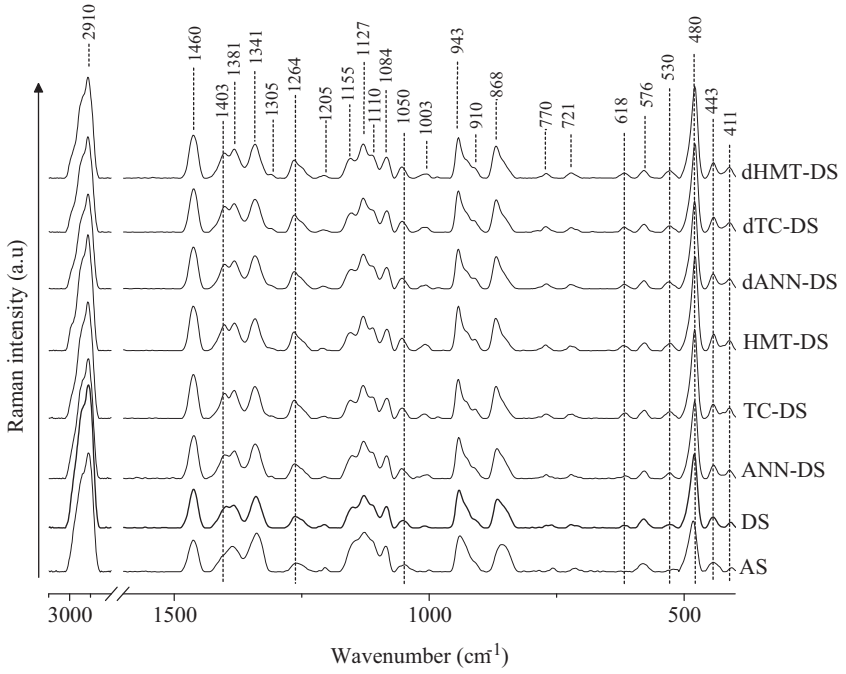

Fig. 5. FT-Raman spectra of amorphous starch (AS), debranched starch (DS), annealed debranched starch (ANN-DS), temperature-cycled debranched starch (TC-DS), heat-moisture treated debranched starch (HMT-DS), and the digested forms: dANN-DS, dTC-DS and dHMT-DS. Broken lines cutting through all spectra mark bands whose intensities show marked crystallinity dependence.

3.3. Correlation of crystallinity with features in Raman spectra

FT-Raman spectra of the various starch preparations are presented in Fig. 5, whereas the assignments to bands are summarized in Table 2. The band at about 865 cm^{-1} was used as internal standard to normalize the spectra for sample size. This band is assigned to symmetric C(1)–O–C(5) stretching (breathing mode) of the α-D-glucose ring (Cael, Koenig, & Blackwell, 1975), whose intensity should not be influenced by the preparation of the starch samples. A number of band dissimilarities are discernible including splitting, sharpening, relative heights, and wavenumber at maximum heights (σ_{Hmax}). Overlaid profiles of some bands are shown in Fig. 6a.

Splitting of the band at 1381 cm^{-1}, usually assigned to δ(C–OH) and δ(C–H) modes (Cael et al., 1973) generated a shoulder at 1403 cm^{-1} assigned to δ(C–H). The prominence of this shoulder increased with increasing starch crystallinity, implying crystallinity-dependent decoupling of the deformational modes (C–H and C–OH) at 1381 cm^{-1}. Similarly the shoulder at 1155 cm^{-1} associated with α-(C1–O–C4′) asymmetric stretch (Sekkal, Dincq, Legrand, & Huvenne, 1995), as well as the shoulder at 1110 cm^{-1} related to C–C, C–H and C–O modes became more prominent due to splitting of the complex band in the 1175–1095 cm^{-1} region.

Band sharpening is evident for the bands at 1264 cm^{-1}, 943 cm^{-1}, 865 cm^{-1} and 480 cm^{-1}, which are related to $\delta(CH_2)$, υ_s(C1–O–C4′), υ_s(C1–O–C5), and skeletal (C–C–O) modes, respectively (Cael et al., 1973). The respective σ_{Hmax} of these bands also shifted markedly with increasing crystallinity. The σ_{Hmax} of the (C–C–O) band at 480 cm^{-1} shifted to a lower value ($r = 0.95$; $p < 0.001$; $n = 8$). A shift of this band towards a higher wavenumber was previously reported during starch gelatinization (Fechner et al., 2005). Likewise, the σ_{Hmax} of the bands at 1264 cm^{-1}, 865 cm^{-1} and 943 cm^{-1} shifted to higher values ($r = 0.98$, 0.96, and 0.96, respectively). The bands at 1264 cm^{-1} and 943 cm^{-1} were reported to shift to lower wavenumbers following transformation of amylose from V- to B-form in a mechanism involving dissociation of the CH_2OH mediated intra-chain bridges due to uptake of water (Cael et al., 1973). Such a mechanism also occurs during starch gelatinization (Schuster et al., 2000). From the XRD reflections of the starches (Fig. 1), contribution by V-structures is not the cause of the shifts of these bands to higher wavenumbers in our case. Instead, an increase in crystallinity arising from helicalization and stabilization of the double helical polymers via intra-chain hydrogen bonding is a more plausible explanation.

Band widths (full width at half maximum height, FWHM) may also provide a measure of the structural variation between samples, whereby, band narrowing is indicator for a narrower distribution of bond energies in the more ordered specimens (Bulkin et al., 1987). This parameter was correlated with crystallinity in the relatively strong bands at 2910 cm^{-1}, 1264 cm^{-1}, 943 cm^{-1}, 865 cm^{-1}, and 480 cm^{-1}. With increasing starch crystallinity, FWHM declined in these bands. For $n = 8$, the correlation coefficients (r) were 0.93 ($p < 0.001$), 0.82 ($p < 0.05$), 0.89 ($p < 0.01$), 0.89 ($p < 0.01$) and 0.98 ($p < 0.001$), respectively. Bulkin et al. (1987) and Fechner et al. (2005) observed similar narrowing of the bands at 2910 cm^{-1} and 480 cm^{-1} in starch gels undergoing retrogradation. From our results, FWMH is most linearly responsive to crystallinity in the skeletal mode band at 480 cm^{-1}. Elsewhere, the 480 cm^{-1} band was reported to become narrower in the spectra of malto-oligosaccharides as the chain length increased to ~60 glycosyl units beyond which no further change occurred (Bulkin et al., 1987). This chain-length effect was seemingly insignificant with our samples.

The υ(C–H) band at 2910 cm^{-1} also gave a relatively strong correlation between FWHM and crystallinity ($r = 0.93$; $p < 0.001$; $n = 8$), an indicator that C–H stretching modes are fairly sensitive to conformational order and packing of polymer chains (Bulkin et al., 1987). However, the correlation coefficient was slightly lower as compared to that of the (C–C–O) band at 480 cm^{-1} ($r = 0.98$; $p < 0.001$; $n = 8$), probably because the υ(C–H) band is a collection of signals arising from symmetric and asymmetric stretching modes of the methylene group (Cael et al., 1973), and possibly also from contributions of Fermi resonance between the overtone of CH_2 deformation and stretching fundamentals (Bulkin et al., 1987).

Table 2
Positions of Raman bands and their assignments.

Band (cm^{-1})	Assignment	Reference
2910	υ(C–H)	a–c
1460	$\delta_s(CH_2)$ twisting, C–H bending	a, b, d
1403 (shoulder)	δ(C–H) bending	j
1381	δ(C–OH), δ(CH) bending, $\delta(CH_2)$ scissoring	a–c
1341	$\delta(CH_2)$ twisting, δ(C–OH) bending	a, b, d, e
1305	δ(C–H)	a
1264	$\delta(CH_2)$, C–OH, CH_2OH (side chain) related mode	a, b, d
1205	δ(C–H)	a
1155 (shoulder)	υ_a(C1–O–C4′) α-(1→4) glycosidic linkage	d
1127	υ(C–OH), δ(C–OH), υ(C–O),	a–d
1110 (shoulder)	C–C, C–O, C–H related modes	a, b
1084	δ(C–OH) bending	a–c
1053	υ(C–OH), δ(C–OH) modes, υ(C–C)	a–d
1003	CH_2 related mode	a, h
943	υ_s(C1–O–C4′)	a–c, f
910 (shoulder)	δ(C–OH), $\delta(CH_2)$, δ(C1–H)	a–d
865	υ_s(C1–O–C5), $\delta(CH_2)$, δ(C–H)	a–c, f
770	υ(C–C) ring mode	a, e
721	υ(C–C) ring mode	a, b e
411, 443, 480, 530, 576, 618	υ(C–C–O), δ(C–C–O) pyranose ring skeletal modes	a–c, g

δ: mode involves change of bond angle (deformation); υ: mode involves change of bond length (stretching). Subscript "*s*": symmetrical; subscript "*a*": asymmetrical.
Key to references: (a) Cael et al. (1973); (b) Santha et al. (1990); (c) Schuster et al. (2000); (d) Sekkal et al. (1995); (e) Kizil et al. (2002); (f) Passauer et al. (2010); (g) de Veij et al. (2009).

The moderately strong correlations between crystallinity and FWHM of the υ_s(C1–O–C4′) and υ_s(C1–O–C5) bands at 943 cm^{-1} and 865 cm^{-1}, respectively ($r = 0.89$; $p < 0.01$ in both cases) may be explained in terms of double helix formation. Orientation of the starch polymers into helical forms coincides with a chain twist about α-(1→4) glycosidic bonds, and the characteristic torsion angles impose a strain-related loss of the stretching symmetry of C1–O–C4′ atoms responsible for the band at ~943 cm^{-1} (Cael et al., 1973; Sekkal et al., 1995). Similarly, increasing chain helicalization progressively alters the orientation of glycosyl units and therefore the symmetry of C(1)–O–C(5) stretch, as well as the coupled deformations of C(1)–H, C(5)–H and C(6)–H_2 groups (Cael et al., 1975). The relatively weaker correlation between FWHM and crystallinity at the 1264 cm^{-1} band ($r = 0.82$; $p < 0.05$; $n = 8$) is probably because

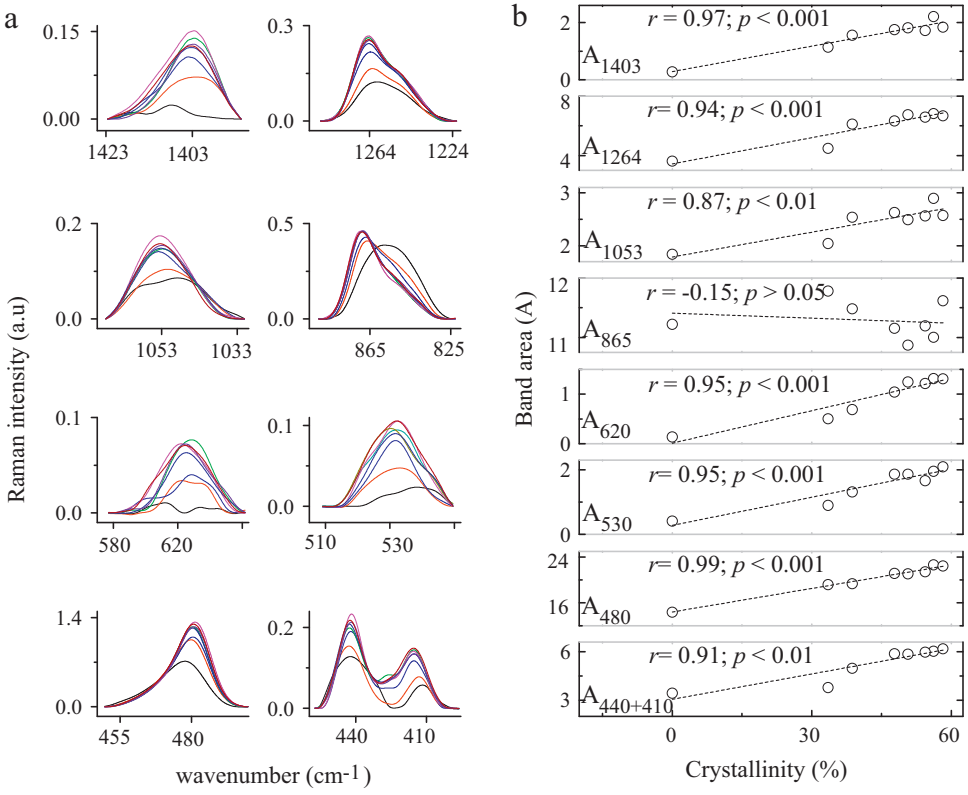

Fig. 6. Overlaid profiles of selected Raman bands of amorphous starch AS (black), debranched starch DS (red), annealed debranched starch ANN-DS (blue), temperature-cycled debranched starch TC-DS (green), heat-moisture treated debranched starch HMT-DS (magenta), and the partially digested forms: dANN-DS (navy), dTC-DS (violet), and dHMT-DS (brown) (a), and linear correlations between crystallinity and band areas (b). The 865 cm^{-1} band was used as internal standard and the band areas (A_{865}) are relatively invariable in the different samples. (For interpretation of the references to color in this figure legend, the reader is referred to the web version of the article.)

vibrations in this region also involve C–OH related modes, meaning that the hydration degree of specimens might have confounding effects.

An advantage of using FWHM for spectral evaluation is that FWHM is a true spectroscopic parameter that is not proportional to concentration, and is less affected by the amount of sample and other experimental variables. However, weak bands that might provide precise relations because they arise from more independent modes are difficult to accurately appraise using this parameter. To incorporate these weak modes in our spectral evaluation, band areas were integrated. Correlations of areas of selected bands and starch crystallinities are shown in Fig. 6b.

Areas of C–C–O band at 480 cm^{-1} gave the best correlation with starch crystallinities ($r = 0.99$; $p < 0.001$; $n = 8$). This band, which is assigned to symmetric vibrations of the glucopyranose ring (Cael et al., 1973), is characteristically strong in starch as compared to other polysaccharides (de Veij et al., 2009). Areas of some other bands also correlated well with starch crystallinity. Schuster et al. (2000) have reported that Raman intensities of the majority of modes including (C–C–O) at 480 cm^{-1} and 530 cm^{-1}; δ(C–OH) and δ(C–H) at 910 cm^{-1}; υ_s(C1–O–C4′) at 943 cm^{-1}; υ(C–OH) and δ(C–OH) at 1053 cm^{-1}; δ (C–OH) at 1084 cm^{-1}; υ(C–OH) and δ (C–OH) at 1127 cm^{-1}; δ(C–OH) and δ(C–H) at 1384 cm^{-1}; υ(C–H) at 2910 cm^{-1}, weaken during starch gelatinization as a result of molecular order loss. We did not find a strong correlation between starch crystallinities and areas of the υ(C–H) band at 2910 cm^{-1}, and this might be attributed to the complex nature of this band.

The bands at 1384 cm^{-1}, 1341 cm^{-1}, 1264 cm^{-1}, 1127 cm^{-1}, 1084 cm^{-1}, and 1053 cm^{-1} are dominated by C–OH modes (Table 2), and the OH groups might contribute to intra-molecular hydrogen bonding between polymer chains. Intra-chain interaction by hydrogen bonding is a characteristic feature of starch crystallization. Intensities of the bands at 1264 cm^{-1} and 1053 cm^{-1}, show direct dependency on crystallinity. However, sensitivity to variations in degree of hydration, possible differences in strengths of intra-chain hydrogen bonding among the starches, or polymorphic differences (Cael et al., 1973) might explain the slightly lower correlation coefficients (Fig. 6b) as compared to that of the skeletal mode band at 480 cm^{-1}. Correlation of crystallinities with areas of the δ(C–H) shoulder at 1403 cm^{-1} was also strikingly strong (Fig. 6b) suggesting crystallinity induced decoupling of the C–H and C–OH motions responsible for the broader band at 1381 cm^{-1}. Areas of skeletal-mode bands at 620, 530, 440, and 410 cm^{-1}, also correlated strongly with sample crystallinities, which we attributed to glucopyranose ring stabilization in crystalline domains.

4. Conclusion

In this study, we evaluated correlations between features in Raman signals and crystallinity of some starch powders. We have shown that there exist strong linear correlations between crystallinity and the Raman signals. With appropriate standardization, integrated areas of Raman bands can be used to generate calibration functions for determination of actual crystallinity values. The isolated skeletal mode at 480 cm^{-1}, which is strong and fairly symmetrical, appears to be the best for this purpose. However, intensity of this band might be influenced by polymer chain length. This suggests that chain-length distribution or amylose and amylopectin content might affect the integrated intensity, and so a calibration function based on this band may be limited to starches of comparable chain-length structure. Intensities of other bands particularly involving skeletal modes are also crystallinity sensitive. It remains necessary to evaluate these modes to establish how they relate to crystallinity in specimens of relatively diverse polymer-chain characteristics.

Acknowledgements

C.M. is grateful to Deutscher Akademischer Austauschdienst (DAAD) for financial support. The authors thank Dr. Thomas Doert and Dr. Silvia Paasch, Department of Chemistry, Technische Universitaet Dresden Germany, for assistance with X-ray diffraction and nuclear magnetic resonance spectroscopy measurements.

References

Buleon, A., Veronese, G., & Putaux, J. L. (2007). Self-association and crystallization of amylose. *Australian Journal of Chemistry*, *60*, 706–718.

Bulkin, B. J., Kwak, Y., & Dea, I. C. M. (1987). Retrogradation kinetics of waxy-corn and potato starches—A rapid, Raman-spectroscopic study. *Carbohydrate Research*, *160*, 95–112.

Cael, J. J., Koenig, J. L., & Blackwell, J. (1973). Infrared and Raman spectroscopy of carbohydrates. Part III. Raman-spectra of polymorphic forms of amylose. *Carbohydrate Research*, *29*, 123–134.

Cael, J. J., Koenig, J. L., & Blackwell, J. (1975). Infrared and Raman-spectroscopy of carbohydrates. Part VI. Normal coordinate analysis of V-amylose. *Biopolymers*, *14*, 1885–1903.

Cairns, P., Bogracheva, T. Y., Ring, S. G., Hadley, C. L., & Morris, V. J. (1997). Determination of the polymorphic composition of smooth pea starch. *Carbohydrate Polymers*, *32*, 275–282.

de Veij, M., Vandenabeele, P., De Beer, T., Remonc, J. P., & Moens, L. (2009). Reference database of Raman spectra of pharmaceutical excipients. *Journal of Raman Spectroscopy*, *40*, 297–307.

Dupuy, N., & Laureyns, J. (2002). Recognition of starches by Raman spectroscopy. *Carbohydrate Polymers*, *49*, 83–90.

Fechner, P. M., Wartewig, S., Kleinebudde, P., & Neubert, R. H. (2005). Studies of the retrogradation process for various starch gels using Raman spectroscopy. *Carbohydrate Research*, *340*, 2563–2568.

Gernat, C., Radosta, S., Anger, H., & Damaschun, G. (1993). Crystalline parts of three different conformations detected in native and enzymatically degraded starches. *Starch-Starke*, *45*, 309–314.

Gidley, M. J., & Bociek, S. M. (1988). ^{13}C CP/MAS NMR-studies of amylose inclusion complexes, cyclodextrins, and the amorphous phase of starch granules—Relationships between glycosidic linkage conformation and solid-state ^{13}C chemical-shifts. *Journal of the American Chemical Society*, *110*, 3820–3829.

Hermans, P. H., & Weidinger, A. (1948). Quantitative X-ray investigations on the crystallinity of cellulose fibers—A background analysis. *Journal of Applied Physics*, *19*, 491–506.

Imberty, A., Buleon, A., Tran, V., & Perez, S. (1991). Recent advances in knowledge of starch structure. *Starch-Starke*, *43*, 375–384.

Kim, I. H., Yeh, A. I., Zhao, B. L., & Wang, S. S. (1989). Gelatinization kinetics of starch by using Raman-spectroscopy. *Biotechnology Progress*, *5*, 172–174.

Kizil, R., Irudayaraj, J., & Seetharaman, K. (2002). Characterization of irradiated starches by using FT-Raman and FTIR spectroscopy. *Journal of Agricultural and Food Chemistry*, *50*, 3912–3918.

Lopez-Rubio, A., Flanagan, B. M., Gilbert, E. P., & Gidley, M. J. (2008). A novel approach for calculating starch crystallinity and its correlation with double helix content: A combined XRD and NMR study. *Biopolymers*, *89*, 761–768.

Ma, C. Y., & Phillips, D. L. (2002). FT-Raman spectroscopy and its applications in cereal science. *Cereal Chemistry*, *79*, 171–177.

Mutungi, C., Onyango, C., Doert, T., Paasch, S., Thiele, S., Machill, S., Jaros, D., & Rohm, H. (2011). Long- and short-range structural changes of recrystallised cassava starch subjected to *in vitro* digestion. *Food Hydrocolloids*, *25*, 477–485.

Mutungi, C., Onyango, C., Jaros, D., Henle, T., & Rohm, H. (2009). Determination of optimum conditions for enzymatic debranching of cassava starch and synthesis of resistant starch type III using central composite rotatable design. *Starch-Starke*, *61*, 367–376.

Mutungi, C., Rost, F., Onyango, C., Jaros, D., & Rohm, H. (2009). Crystallinity, thermal and morphological characteristics of resistant starch type III produced by hydrothermal treatment of debranched cassava starch. *Starch-Starke*, *61*, 634–645.

Paris, M., Bizot, H., Emery, J., Buzare, J. Y., & Buleon, A. (1999). Crystallinity and structuring role of water in native and recrystallized starches by ^{13}C CP-MAS NMR spectroscopy. 1. Spectral decomposition. *Carbohydrate Polymers*, *39*, 327–339.

Paris, M., Bizot, H., Emery, J., Buzare, J. Y., & Buleon, A. (2001). NMR local range investigations in amorphous starchy substrates. I. Structural heterogeneity probed by ^{13}C CP-MAS NMR. *International Journal of Biological Macromolecules*, *29*, 127–136.

Passauer, L., Bender, H., & Fischer, S. (2010). Synthesis and characterisation of starch phosphates. *Carbohydrate Polymers*, *82*, 809–814.

Phillips, D. L., Xing, J., Chong, C. K., Liu, H. J., & Corke, H. (2000). Determination of the degree of succinylation in diverse modified starches by Raman spectroscopy. *Journal of Agricultural and Food Chemistry*, *48*, 5105–5108.

Pifferi, G., Santoro, P., & Pedrani, M. (1999). Quality and functionality of excipients. *Farmaco*, *54*, 1–14.

Pohu, A., Planchot, V., Putaux, J. L., Colonna, P., & Buleon, A. (2004). Split crystallization during debranching of maltodextrins at high concentration by isoamylase. *Biomacromolecules*, *5*, 1792–1798.

Sajilata, M. G., Singhal, R. S., & Kulkarni, P. R. (2006). Resistant starch—A review. *Comprehensive Reviews in Food Science and Food Safety*, *5*, 1–17.

Santha, N., Sudha, K. G., Vijayakumari, K. P., Nayar, V. U., & Moorthy, S. N. (1990). Raman and infrared-spectra of starch samples of sweet-potato and cassava. *Proceedings of the Indian Academy of Sciences-Chemical Sciences*, *102*, 705–712.

Schuster, K. C., Ehmoser, H., Gapes, J. R., & Lendl, B. (2000). On-line FT-Raman spectroscopic monitoring of starch gelatinisation and enzyme catalysed starch hydrolysis. *Vibrational Spectroscopy*, *22*, 181–190.

Sekkal, M., Dincq, V., Legrand, P., & Huvenne, J. P. (1995). Investigation of the glycosidic linkages in several oligosaccharides using FT-IR and FT-Raman spectroscopies. *Journal of Molecular Structure*, *349*, 349–352.

Tan, I., Flanagan, B. M., Halley, P. J., Whittaker, A. K., & Gidley, M. J. (2007). A method for estimating the nature and relative proportions of amorphous, single, and double-helical components in starch granules by ^{13}C CP/MAS NMR. *Biomacromolecules*, *8*, 885–891.

Tester, R. F., Karkalas, J., & Qi, X. (2004). Starch—Composition, fine structure and architecture. *Journal of Cereal Science*, *39*, 151–165.

Thygesen, L. G., Lokke, M. M., Micklander, E., & Engelsen, S. B. (2003). Vibrational microspectroscopy of food. Raman vs. FT-IR. *Trends in Food Science and Technology*, *14*, 50–57.

van Soest, J. J. G., Tournois, H., deWit, D., & Vliegenthart, J. F. G. (1995). Short-range structure in (partially) crystalline potato starch determined with attenuated total reflectance Fourier-transform IR spectroscopy. *Carbohydrate Research*, *279*, 201–214.

Wellner, N., Georget, D. M. R., Parker, M. L., & Morris, V. J. (2011). In situ Raman microscopy of starch granule structures in wild type and *ae* mutant maize kernels. *Starch-Starke*, *63*, 128–138.